Monitoring of radiofrequency thermal ablation in liver tissue through fibre Bragg grating sensors array

D. Tosi, E.G. Macchi, G. Braschi, M. Gallati, A. Cigada, S. Poeggel, G. Leen and E. Lewis

A fibre Bragg grating (FBG) array-based sensing probe has been installed on a device for radiofrequency thermal ablation (RFTA). The probe is made of five FBGs with 0.5 cm active area and 1 cm spacing, to provide quasi-distributed thermal pattern measurements. Multiple experiments have been conducted on porcine liver, reporting the temperature pattern along the ablation axis. Thermal maps allow an estimation of the RFTA efficiency and spatial extension in the liver.

Introduction: Radiofrequency thermal ablation (RFTA) is a medical procedure for post-screening treatment of lung, hepatic and kidney tumours via hyperthermia [1]. The concept of RFTA is to exploit RF irradiance to generate a well-confined high-temperature region at the focal point of the tumour. Heat is generated by RF irradiance from a thin RFTA needle (1–4 mm, percutaneous) to the target and then propagated by conduction in a symmetrical way. The mortality rate of tumour cells is a function of temperature value and its persistence: temperatures higher than 42°C are cytotoxic [2], whereas 52°C for 1 min is a typical reference value; over 60°C cell death is nearly instantaneous. As the real-time thermal profile in the ablated region plays a fundamental role in the tumour cell mortality, the quasi-distributed measurement of temperature in the tissue throughout the ablation is a key asset. Previous literature shows thermal measurements with a thermocouple [3], which, however, alters both the RF irradiance and the tissue, and with an infrared thermal camera [4], which, however, requires a line of sight with the ablation region, typically unavailable in RFTA.

In this Letter, we report the thermal measurement of the RFTA pattern in porcine liver, based on a fibre Bragg grating (FBG) array [5, 6]. The FBG array has been directly mounted on the ablation device, providing real-time temperature measurement at 5 points (1 sensor/cm).

Setup: The RFTA setup is illustrated in Fig. 1. A medically-certified RF generator is used to power the electrical circuit with 20 W power and 480 kHz carrier; this device embeds an impedance meter that forces a stop in power supply when impedance is >300 Ω. RF power is monitored online with an oscilloscope. The RFTA device is a hollow needle with 4 mm outer diameter. Porcine liver tissue is used as phantom, positioned on a metallic layer serving as the second electrode. The fibre-optic probe is an FBG array based on draw-tower fabrication on ormocer coating (195 µm diameter), provided by the FBGS Technologies. The FBG array has a uniform spectral spacing (1.8 nm between each Bragg wavelength, 1546.0–1553.2 nm) and a uniform geometrical distribution (0.5 cm active area, 1 cm between each FBG centre). The thermo-optic FBG coefficient is 11.66 pm/°C. Interrogation is performed with a white-light setup based on a broadband source (Opto-Link ASE, 20 mW), a 3 dB coupler and a spectrometer (Ibsen I-MON).

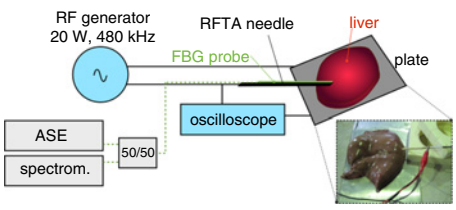

Fig. 1 *Setup of RFTA with FBG sensing system*

A simple packaging has been used as shown in Fig. 2. The FBG array has been attached to the RFTA needle by means of adhesive tape at two points. The first sealing point lies outside of the FBG array, while the second fastening point is in the middle of the FBG array. To create a reference point and to provide additional protection for the insertion, the needle tip and FBG5 are coated with insulating tape. The electrical insulation between the RFTA needle and the liver tissue leaves a region of 1.9 cm length which directly irradiates the RF signal to the liver, whereas the tip and the tail of the needle are more insulated. As a consequence, FBG4 is the closest sensor to the ablation peak and FBG5 and FBG3, partially insulated by the tape, lie at +1 and −1 cm, respectively; FBG2 and FBG1 are located at the tail of the FBG array.

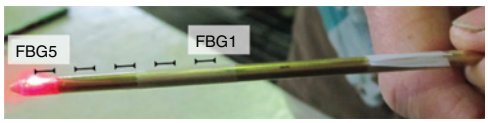

Fig. 2 *Picture of FBG probe mount on 4 mm RFTA needle*

Results and discussion: Fig. 3 shows the temperature recorded by each FBG during an RFTA procedure. After the initialisation, the temperature recorded in the proximity of the peak (FBG3-5) rises up to 48–55°C after 25 s, whereas FBG2 records 28°C and FBG1 measures 20°C. After the initial fast growth, the temperature rises almost linearly from 25 to 155 s. FBG4, positioned at the ablation peak, records the highest temperature, followed by FBG5 and FBG4, which record similar temperature values, slightly different possibly due to the packaging and a slight asymmetry in the RF irradiance. At 150 s, FBG5 records 106°C, whereas FBG4 measures 121°C, hence showing a spatial gradient of 15°C/cm. The approximate slope of FBG5 and FBG4, between 25 and 150 s, is 0.52 and 0.44°C/s, respectively, whereas FBG2 and FBG1 record an approximate rise of 0.25 and 0.16°C/s. When the liver tissue is exposed to temperatures >100°C, a liquid-to-vapour transition is experienced, leading to an abrupt increase of the liver impedance to well over 300 Ω, which neutralises any further ablation. The RF generator automatically stops the power supply after 175 s when reaching a peak value of 138.6°C, and then the temperature rapidly decreases.

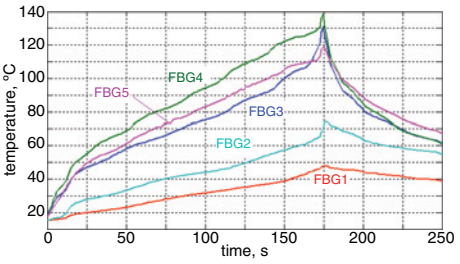

Fig. 3 *Temperature measured for each FBG during RFTA procedure*

To show the role of the FBG array in RFTA, Fig. 4 gives the results of three different ablation experiments, all performed under the same conditions and with the same setup as in Figs. 1 and 2. The Figure shows the thermal maps obtained reporting the estimated temperature along the longitudinal axis; the distance parameter refers to the geometrical distance between each FBG and the centre of FBG4, considered as the ablation peak. The first ablation shows results similar to Fig. 3, whereas the second RFTA has a longer duration (310 s); the third RFTA experiment has a shorter duration, 165 s. Such variability of ablation duration can be attributed to the electrical properties of the liver; although using similar porcine samples, the evolution of liver tissue impedance is different in each procedure and leads to a variability in the RFTA duration. Temperature distributions have been oversampled (1:10 rate) in order to smooth the curves. In all three charts, it is possible to observe the behaviour of Fig. 3. A few seconds after the RFTA start, the temperature exhibits an abrupt increase, with an approximate quadratic shape; then, temperature growth reduces its slope, assuming a nearly linear pattern until reaching the vapourisation phase; then, a final abrupt temperature rise is observed until the RF generator is disconnected. Peak temperatures of 138.5, 133.1 and 131.6°C have been observed. The three charts provide a quantitative determination of the exposure of each portion of the tissue to cytotoxic temperatures, quantifying the exposure time. In the first chart, in particular, we observe that for negative distance the 60°C threshold, which guarantees a high mortality rate, is achieved for a distance inferior to 2.4 cm from the ablation peak. A similar value (2.5 cm) is observed for the second RFTA, whereas the third ablation, despite being the shortest, guarantees an exposure to 58°C or higher all the way through the RFTA needle.

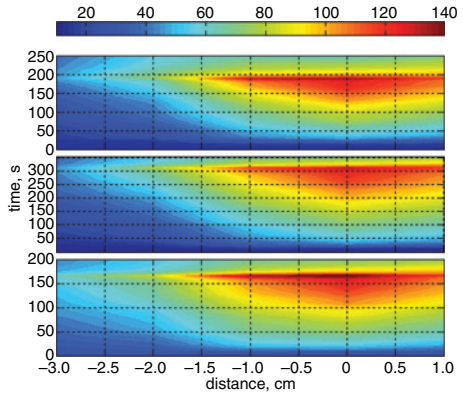

Fig. 4 *Temperature distribution along longitudinal axis for three different RFTA procedures having 20 W RF power, highlighting temperature contours*
Colour-map gives temperature in °C

Fig. 5 reports the thermal profile of the three RFTA experiments on a single chart by normalising both temperature and time in the 0–1 range; for visual clarity, only FBG2 and FBG4 are shown. This analysis allows a post-RFTA analysis of thermal trends, comparing different ablation results. The chart shows that in RFTA2, the longest experiment, the normalised temperature recorded by FBG4 at the ablation peak rises faster than in the other two experiments, whereas at the other end the growth of temperature at the needle tail, recorded by FBG2, has the slowest growth. Conversely, the opposite trend is found for the third experiment, which has the shortest duration: the higher temperature increase recorded by FBG2 in this experiment confirms that the heat distribution has a deeper penetration, providing an effective hyperthermia treatment on a broader area, as confirmed by Fig. 4.

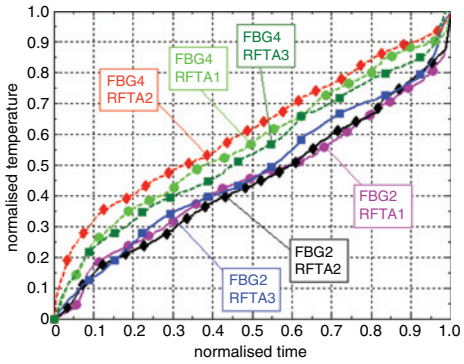

Fig. 5 *Thermal behaviour of three RFTA procedures, considering only temperature rise; both time and temperature values have been normalised*
Figure shows temperature readout for FBG2 (dashed line) and FBG4 (solid line) for each RFTA procedure (in sequence: circle, diamond, square markers).

Conclusions: An FBG array, having 1 sensor/cm density, has been installed on an RFTA needle for online measurement of temperature distribution during the ablation procedure. Measurements performed ex vivo on porcine liver phantom show the capability of the fibre-optic sensors to measure the steep temperature gradient. Thermal maps allow quantifying the exposure of each part of the tissue to the high-temperature field and provide a comparison between different procedures. The achieved results show the possibility of embedding FBG arrays on ablation devices in order to dynamically estimate the efficiency of the procedure and predict the ablation output. Such a result is significant for hepatic tumours, in which the electrical properties of the liver limit the RFTA to tumours up to ~3 cm in size.

Acknowledgments: This work was supported by the Marie Curie action MC-IEF-299985 and the Fondazione per la Cura Mini-Invasiva Tumori. The authors acknowledge the support of FBGS Technologies.

19 February 2014
doi: 10.1049/el.2014.0620
One or more of the Figures in this Letter are available in colour online.

D. Tosi, S. Poeggel, G. Leen and E. Lewis (*Optical Fibre Sensors Research Centre, University of Limerick, Limerick, Ireland*)

E-mail: daniele.tosi@ul.ie

E.G. Macchi, G. Braschi and M. Gallati (*Dipartimento di Ingegneria Civile ed Architettura, Universita' di Pavia, via Ferrata 3, 27100 Pavia, Italy*)

A. Cigada (*Dipartimento di Meccanica, Politecnico di Milano, via La Masa 34, 20158 Milano, Italy*)

References

1 Curley, S.: 'Radiofrequency ablation of malignant liver tumors', *Ann. Surg. Oncol.*, 2003, **1**, pp. 338–347
2 Sapareto, S.A.: 'Thermal dose determination in cancer therapy', *Int. J. Radiat. Oncol. Biol. Phys.*, 1984, **10**, (6), pp. 787–800
3 Dodd, M.J.: 'Radiofrequency ablation of the liver: current status', *Am. J. Roentgen*, 2001, **176**, pp. 3–16
4 Ogan, K., Roberts, W.R., Wilhelm, D.M., Bonnell, L., Leiner, D., Lindberg, G., Kayoussi, L.R., and Cadeddu, J.A.: 'Infrared thermography and thermocouple mapping of radiofrequency renal ablation to assess treatment adequacy and ablation margins', *Urology*, 2003, **62**, pp. 146–151
5 Webb, D.J., Jones, S., Zhang, L., Bennion, I., Hathaway, M.W., and Jackson, D.A.: 'First in-vivo trials of a fiber Bragg grating based temperature profiling system', *J. Biomed. Opt.*, 2000, **5**, (1), pp. 45–50
6 Saccomandi, P., Schena, E., and Silvestri, S.: 'Techniques for temperature monitoring during laser-induced thermo-therapy', *Int. J. Hyperth.*, 2013, **29**, pp. 609–619